JOINT EUROPEAN TORUS

JET–P(92)56

C. Baxi, H.D. Falter
and JET Team

A Model for Analytical Performance Prediction of Hypervapotron

A Model for Analytical Performance Prediction of Hypervapotron

C. Baxi, H.D. Falter
and JET Team*

JET-Joint Undertaking, Culham Science Centre, OX14 3DB, Abingdon, UK

[1]General Atomics, PO Box 85608, San Diego, Ca 29186-9784, USA
** See Annex*

A MODEL FOR ANALYTICAL PERFORMANCE PREDICTION OF HYPERVAPOTRON

C Baxi* and H D Falter**
* General Atomics, PO Box 85608, San Diego, Ca 29186-9784, USA
** JET Joint Undertaking, Abingdon, Oxon OX14 3EA, UK

ABSTRACT

A hypervapotron is a water cooled device which combines the advantages of finned surfaces with the large heat transfer rates possible during boiling heat transfer. Hypervapotrons have been used as beam dumps in the past and plans are under way to use them for the divertor in the Joint European Tokamak (JET). Experiments at JET have shown that a surface heat flux of 25MW/m^2 can be achieved in hypervapotrons. This performance makes this device very attractive for cooling of divertor of the International Thermonuclear Experimental Reactor (ITER). This paper presents an analytical method to predict the thermal performance of the hypervapotron made of materials other than copper. After further development and verification, the analytical method could be used for optimising designs and performance prediction.

1. INTRODUCTION

A hypervapotron consists of a finned surface made of high conductivity material such as copper (Fig.1). The coolant is subcooled water, at a high velocity and high pressure and flows perpendicular to the fins. Miller (ref.1) has discussed the types of possible flows in such a geometry. Experiments (ref.2-3) have shown that the ideal geometry consists of fins with a height to pitch ratio of about 0.5. A recent paper (ref.4) discusses resonant heat transfer in a geometry similar to hypervapotron. However, this study is limited to forced convection flow.

Hypervapotrons have been used at JET as beam dumps in the Neutral Injection Systems to remove large heat fluxes under steady-state conditions. On-going developments are directed towards using these devices with beryllium tiles brazed onto the front surface as divertor target plates. Extensive experiments have been carried out on hypervapotrons at the 10MW JET Neutral Beam Test Bed [refs.2-3]. The test parameters cover a wide range of geometry, pressure, velocity and subcooling. Peak heat fluxes of about 25MW/m^2 have been obtained in these tests.

At low heat fluxes the heat transfer is by forced convection. As the heat flux is increased, some of the surface reaches incipient boiling temperature. With further increase in incident heat flux, critical heat flux conditions will be applicable to a least part of the heat transfer surface. Ultimately, part of the surface will melt. The maximum temperature is a function of water pressure, hypervapotron geometry, velocity of flow, length of hypervapotron, heat flux and coolant inlet temperature.

In this paper an attempt is made to predict the thermal performance of hypervapotrons by combination of heat transfer correlations and finite element analysis. If such an analytical prediction is feasible, designs could be optimised and the performance predicted for untested conditions, materials and geometries.

2. ANALYSIS

2.1 Heat transfer correlations

The heat transfer is in three different regions:

a) Forced convection

The following Modified Dittus Boelter correlation [5] was used for temperatures less than incipient boiling temperature.

$$Nu = 0.023\ (ff)\ (Re)^{0.8}\ (Pr)^{0.33} \qquad (1)$$

The factor ff = 1.35 to account for the re-circulating flow (indicated schematically in Fig.1) which occurs in the channels formed by the fins [3]. This factor was obtained by comparing calculated results with measured results at a variety of flow velocities and geometries at low values of incident heat flux. The hydraulic diameter used in Re and Nu was hydraulic diameter of the channel between the fins (Fig.1).

b) Transition from forced convection to Nucleate boiling

The incipient boiling temperature is the intersection of eq.(1) and Bergles Rosenhow correlation [6].

$$q'' = 1.8\times10^3\, p^{1.156}\,(1.8\Delta T_{sat})^{\frac{2.8}{p^{0.0234}_{ONB}}} \tag{2}$$

c) Nucleate boiling

The nucleate boiling heat flux was calculated by Thom's [7] correlation:

$$q''B = 10^6\,[(e^{\frac{p}{87\times10^5}})(T_W - T_{sat})/22.65]^2 \tag{3}$$

The heat flux for temperatures greater than incipient boiling temperature was calculated by [8].

$$\frac{q''}{q''FC} = \left[1 + \frac{(q''B)^2}{(q''FC)^2}\left(1 - \frac{q''Bi}{q''B}\right)^2\right]^{1/2} \tag{4}$$

d) Critical heat flux was calculated using the Macbeth correlation [9-12];

$$(q''crit \times 10^{-6}) = \frac{A+D(G\times10^{-6})(\Delta i_{sub})i}{C+z}\ , \tag{5}$$

where

$$A = y_0\, Dy_1\, (G\times10^{-6})\, y_2\ , \tag{6}$$

$$C = y_2\, Dy_4\, (G\times10^{-6})\, y_3\ , \tag{7}$$

The constants are listed in ref. 7. This particular correlation was chosen because it takes into consideration effects of geometry and pressure. This correlation is applicable at the relatively low pressures and high velocities in the hypervapotron.

All above correlations require calculation of heat flux as a function of local surface temperature for each set of conditions (Geometry,

Pressure, Coolant bulk temperature and flow rate). Hence all above equations were programmed in a computer code which created the input for the finite element code TOPAZ2D [13]. Figure 2 shows a typical variation of heat transfer co-efficient as a function of local surface temperature in the cooling channel.

2.2 Finite Element Model

The finite element model for the TOPAZ2D code was of half a fin. The incident heat flux, the coolant bulk temperature and heat transfer co-efficients calculated from above procedure were the boundary conditions. The coolant temperature was set equal to coolant temperature at half way along the length of the hypervapotron. A steady-state calculation was performed. The aim was to calculate the temperature distribution in the hypervapotron and to compare experimentally measured surface temperature with analysis.

3. RESULTS

Figures 3 to 5 shows the comparison of this analysis with experiments done at the JET Test Bed on narrow channel (3mm channel height) and wide channel (6mm) hypervapotrons. As seen in Fig.3, the heat transfer has three regions. In the first region, the heat transfer is by forced convection. In the second region, part of the heat transfer surface reaches incipient boiling temperature and hence the heat transfer co-efficient is higher than the forced convection region, thus the slope dTs/dq" is less than in the pure forced convection region. With further increase in heat transfer surface temperature, some of the surface reaches critical heat flux condition described by eq.(4). The heat flux does not increase with further increase in temperature (Fig.2). Thus the heat transfer co-efficient actually decreases with temperature. Due to this, the surface temperature increases rapidly with increasing heat flux. If it was not for the finned surface and large thermal conductivity of the copper, burn-out would have occurred at this time. Increasing heat flux will finally make local heat flux at all locations on the heat transfer surface to the coolant greater than the critical heat flux and burn-out will occur.

Figures 3 to 5 show an excellent agreement between this analysis and experimental results. This analysis covered a wide range of pressures, flow velocities and sub-cooling and two different geometries. In future, an analysis will be performed to see if this model can predict performance of other geometries for which experimental data is available. An attempt could then be made to optimise the design of hypervapotrons for applications to the ITER design.

Figures 6 to 8 show the isotherms in the hypervapotron for three flow regimes. Figure 6 is for a heat flux of $2MW/m^2$ and represents the forced convection regime because the temperatures over the entire heat transfer surface are below incipient boiling temperature. As the surface heat flux is increased to $8MW/m^2$ (Fig.7), part of the surface has nucleate boiling and part of the surface has forced convection. As the heat flux on the surface of the hypervapotron is further increased to $25MW/m^2$, some part of the heat transfer surface reaches the critical heat flux condition (Fig.8). However, burn-out is prevented due to conduction heat transfer to the colder surface. This is the important feature of the hypervapotron where considerably higher heat flux on the surface than the critical heat flux in the coolant channel can be achieved.

The method presented above was used to analyse the performance of hypervapotron for materials other than copper. Figure 9 shows the effect of thermal conductivity of peak surface temperature at a surface heat flux of $25MW/m^2$. The result shows that the surface temperature for a hypervapotron made of materials other than copper will be considerably higher.

4. DISCUSSION

A method has been presented which predicts the thermal performance of hypervapotron. Further work is planned to extend the method to more general geometry. Two specific extensions of the method are envisaged: inclusion of three dimensional effects and calculation of pressure oscillations during boiling.

REFERENCES

1. R Tivey, et al., "Testing of Beam Stopping Elements Using Hypervapotron Cooling", Proc. SOFE, Monterey 1987.

2. H Altmann, et al., "A Comparison Between Hypervapotron and Multitube High Heat Flux Stopping Elements", Proc. SOFE, Knoxville 1989.

3. D S Miller, "Internal Flow systems", BHRA Fluid Engineering 1978.

4. M Greiner, " An Investigation of Resonant Heat Transfer Enhancement in Grooved Channels", Int. J. Heat Mass Transfer, Vol.34, N° 6, pp. 1383-391.

5. W M Rosenhow, et al, editors, "Handbook of Heat Transfer Fundamentals", McGraw-Hill Book Co, New York, 1983.

6. A E Bergles and W M Rosenhow, "The determination of forced convection surface boiling heat transfer", paper 63-HT-22. Paper presented at the 6th National Heat Transfer Conference of the ASME-AIChE held at Boston, (11-14 August 1963).

7. J R S Thron, W M Walker, T A Fallon and G F S Reising, "Boiling in Subcooled Water during Flow in Tubes and Annuli", Proc. Inst. Mech. Eng. (3C)180:226 (1965-1966).

8. A E Bergles and W M Rosenhow, J. Heat Transfer, 86:365 (1964).

9. B Thompson and R V Macbeth, "Boiling water heat transfer – burn-out in uniformly heated round tubes: A compilation of world data with accurate correlations", AEEW-R 356 (1964).

10. R V Macbeth, "Burn-out analysis", Part 4, "Application of a local condition pothesis to world data for uniformly heated round tubes and rectangular channels", AEEW-R 267 (1963).

11. R V Macbeth, "Burn-out analysis", Part 3, "The low velocity burn-out regime", AEEW-R 222 (1963).

12. J G Collier, "Convective Boiling and Condensation", McGraw-Hill, New York.

13. A B Shapiro, "TOPAZ - A finite Element Heat Conduction Code", UCID-20045, March 1984.

NOMENCLATURE

D	=	hydraulic diameter of the flow channel without fins, m
ff	=	factor, Eq.(1)
G	=	mass flux, kg/m^2-sec
h	=	heat transfer co-efficient, W/m^2-°C
i	=	enthalpy, kJ/kg
K	=	thermal conductivity, W/m-°C
Nu	=	Nusselt number = hD/K
p	=	pressure, Pa
Pr	=	Prandtl number
q''	=	heat flux in cooling channel, MW/m^2
Q''	=	incident heat flux, MW/m^2
Re	=	Reynolds number
T	=	temperature °C
V	=	velocity, m/sec
Z	=	length, m
ΔT	=	temperature difference, °C
Δi	=	enthalpy difference, kJ/kg

Subscripts

b	=	bulk
B	=	boiling
Bi	=	incipient boiling
CRIT	=	critical
FC	=	forced convection
ONB	=	onset of boiling
SAT	=	saturated
W	=	wall

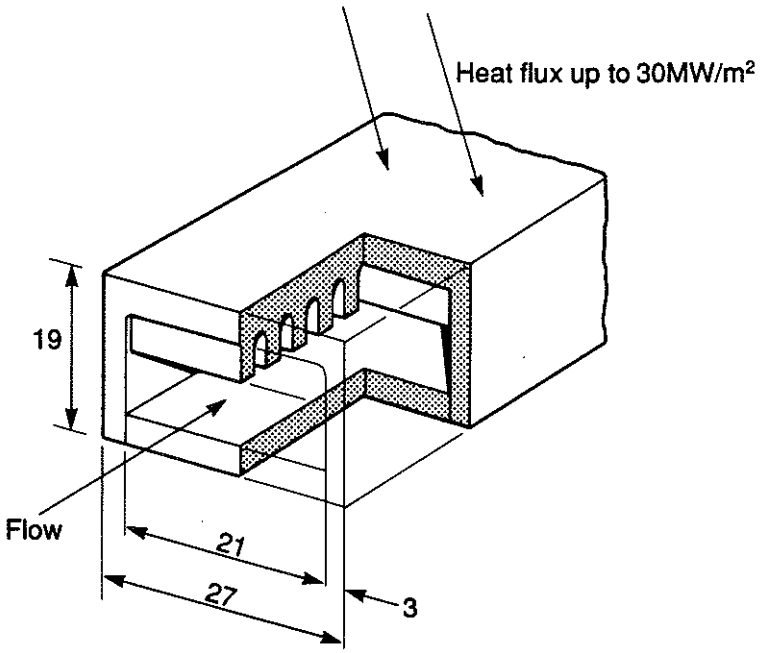

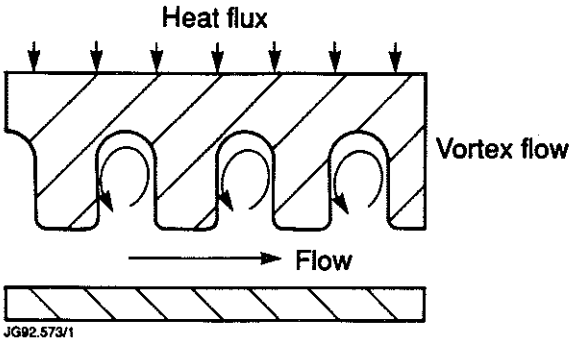

Fig. 1 Hypervapotron

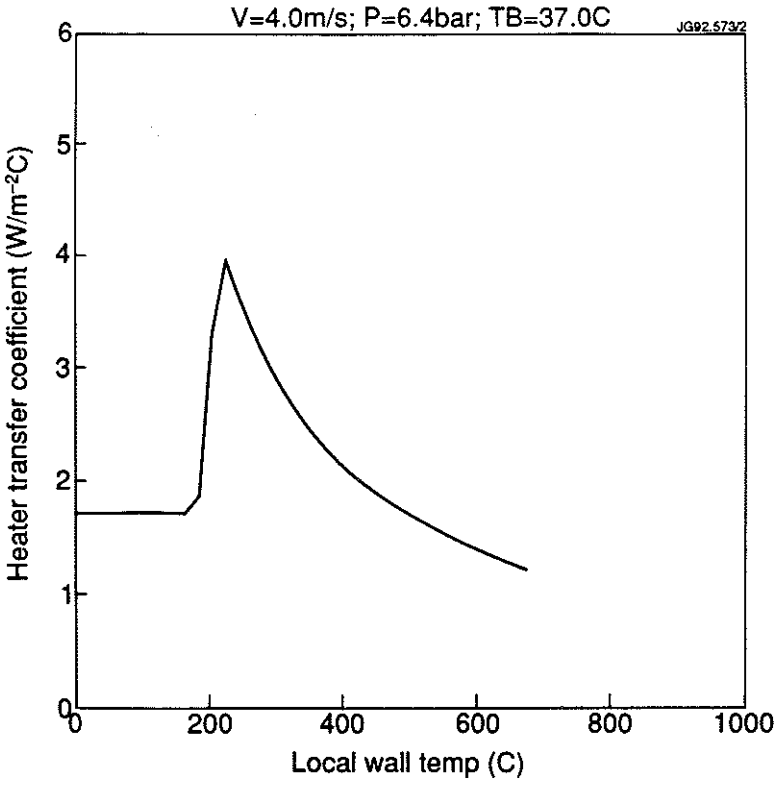

Fig. 2 Heat transfer coefficient for 6mm channel V=4.0m/s; P=6.4bar; TB=37.0C

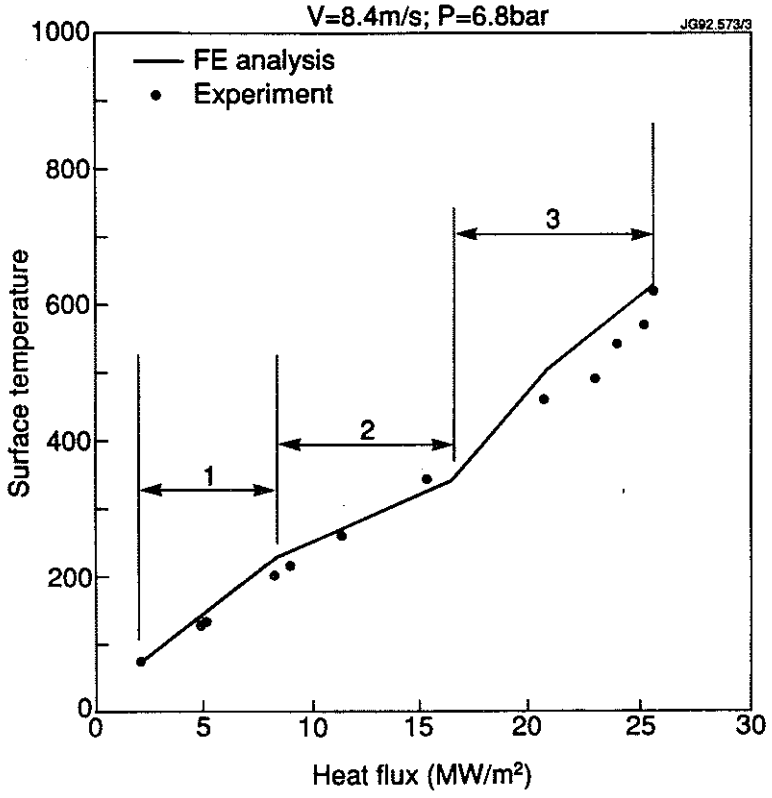

Fig.3 Comparison of analysis and experiment for narrow channel vapotronV=8.4m/s; P=6.8bar

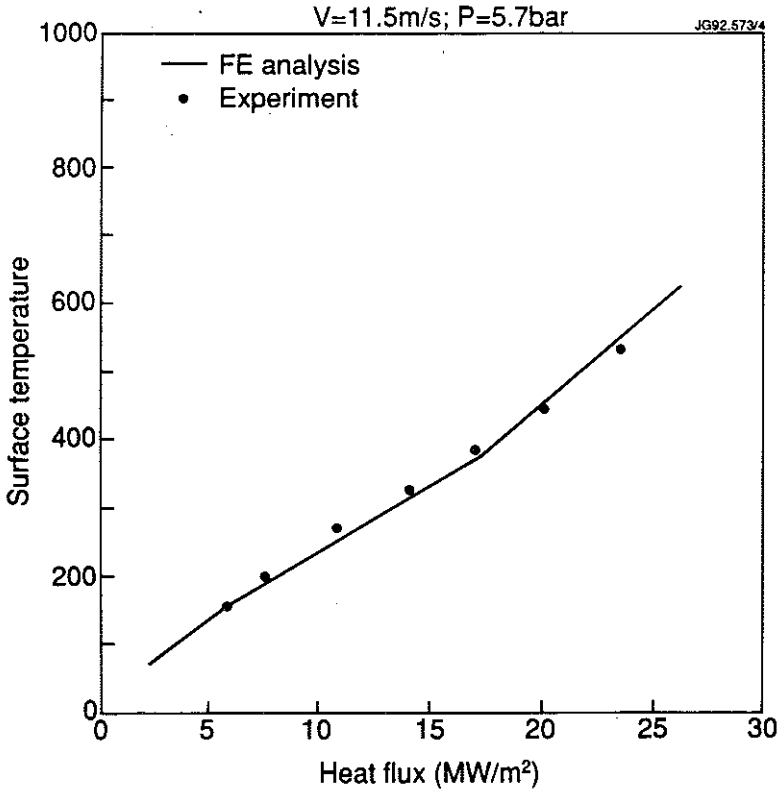

Fig. 4 Comparison of analysis and experiment for narrow channel vapotron V=11.5m/s; P=5.7bar

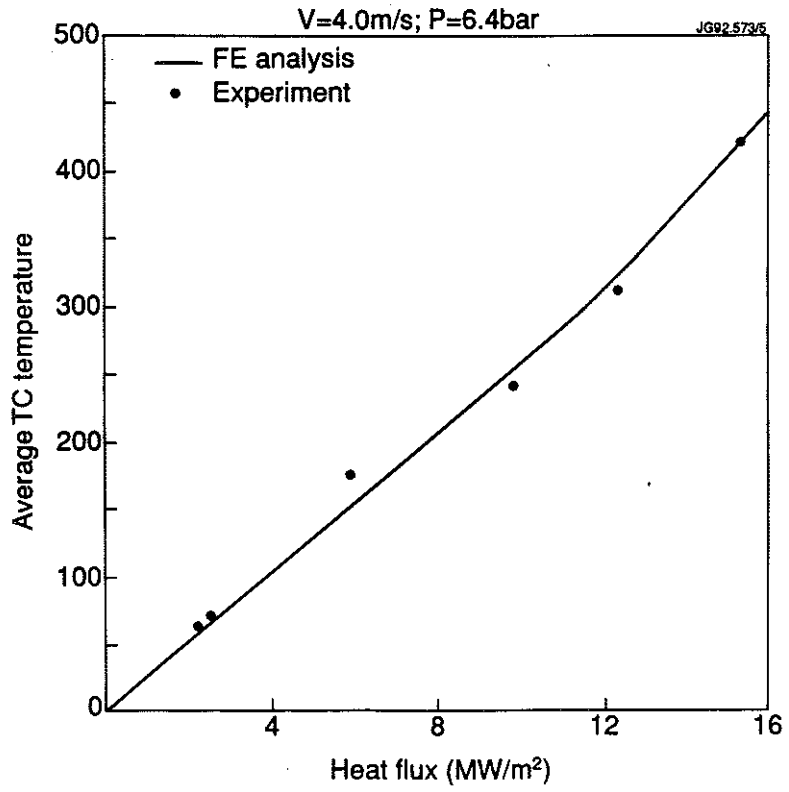

Fig.5 Comparison of analysis and experiment for wide channel (6mm) vapotron V=4.0m/s; P=6.4bar

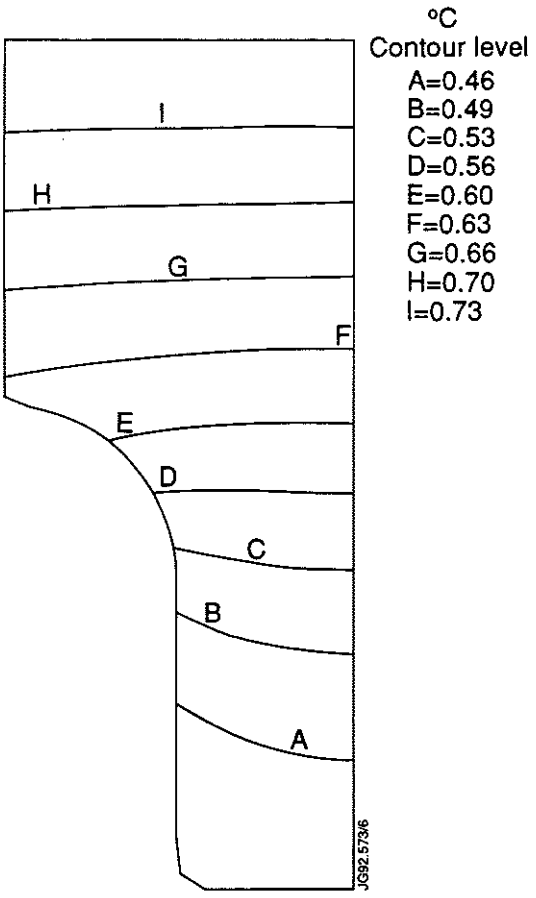

Fig. 6 Isotherms (°C) for forced convection regime (heat flux=2MW/m²)

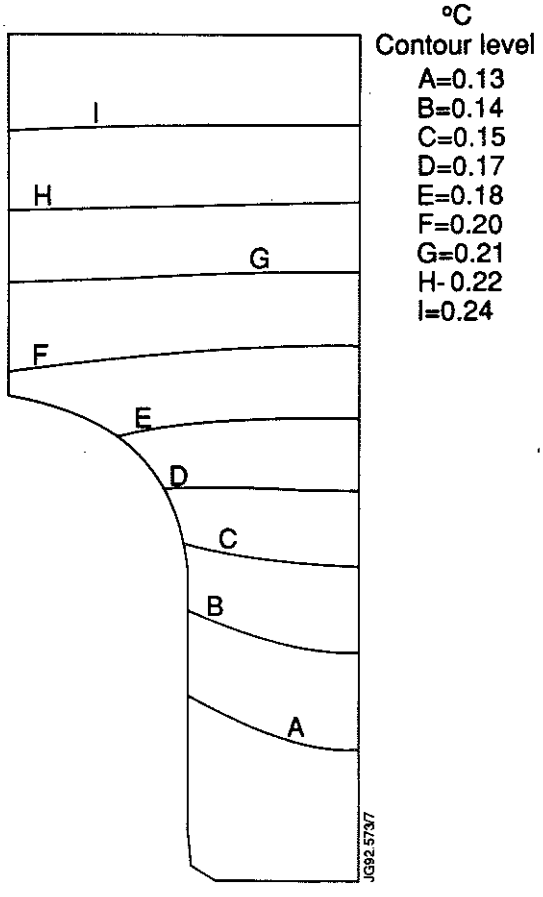

Fig 7. Nucleate boiling regime (Heat flux=8MW/m²)

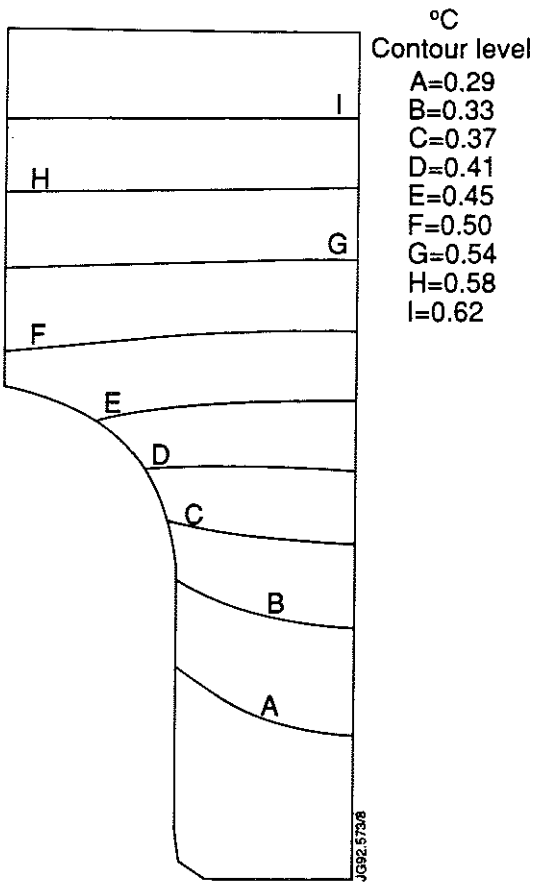
°C
Contour level
A=0.29
B=0.33
C=0.37
D=0.41
E=0.45
F=0.50
G=0.54
H=0.58
I=0.62
I
H
G
F
E
D
C
B
A
JG92.573/8

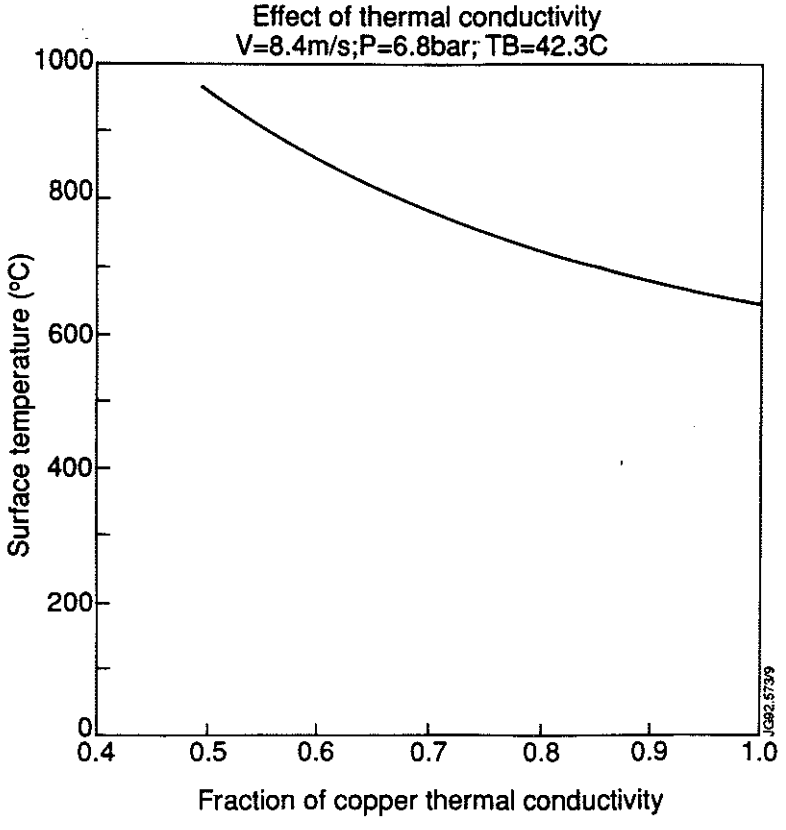
Effect of thermal conductivity
V=8.4m/s;P=6.8bar; TB=42.3C
Surface temperature (°C)
1000
800
600
400
200
0
0.4
0.5
0.6
0.7
0.8
0.9
1.0
Fraction of copper thermal conductivity
JG92.573/9

Appendix I

THE JET TEAM

JET Joint Undertaking, Abingdon, Oxon, OX14 3EA, U.K.

J.M. Adams[1], B. Alper, H. Altmann, A. Andersen[14], P. Andrew, S.Ali-Arshad, W. Bailey, B. Balet, P. Barabaschi, Y. Baranov, P. Barker, R. Barnsley[2], M. Baronian, D.V. Bartlett, A.C. Bell, G. Benali, P. Bertoldi, E. Bertolini, V. Bhatnagar, A.J. Bickley, D. Bond, T. Bonicelli, S.J. Booth, G. Bosia, M. Botman, D. Boucher, P. Boucquey, M. Brandon, P. Breger, H. Brelen, W.J. Brewerton, H. Brinkschulte, T. Brown, M. Brusati, T. Budd, M. Bures, P. Burton, T. Businaro, P. Butcher, H. Buttgereit, C. Caldwell-Nichols, D.J. Campbell, D. Campling, P. Card, G. Celentano, C.D. Challis, A.V.Chankin[23], A. Cherubini, D. Chiron, J. Christiansen, P. Chuilon, R. Claesen, S. Clement, E. Clipsham, J.P. Coad, I.H. Coffey[24], A. Colton, M. Comiskey[4], S. Conroy, M. Cooke, S. Cooper, J.G. Cordey, W. Core, G. Corrigan, S. Corti, A.E. Costley, G. Cottrell, M. Cox[7], P. Crawley, O. Da Costa, N. Davies, S.J. Davies[7], H. de Blank, H. de Esch, L. de Kock, E. Deksnis, N. Deliyanakus, G.B. Denne-Hinnov, G. Deschamps, W.J. Dickson[19], K.J. Dietz, A. Dines, S.L. Dmitrenko, M. Dmitrieva[25], J. Dobbing, N. Dolgetta, S.E. Dorling, P.G. Doyle, D.F. Düchs, H. Duquenoy, A. Edwards, J. Ehrenberg, A. Ekedahl, T. Elevant[11], S.K. Erents[7], L.G. Eriksson, H. Fajemirokun[12], H. Falter, J. Freiling[15], C. Froger, P. Froissard, K. Fullard, M. Gadeberg, A. Galetsas, L. Galbiati, D. Gambier, M. Garribba, P. Gaze, R. Giannella, A. Gibson, R.D. Gill, A. Girard, A. Gondhalekar, D. Goodall[7], C. Gormezano, N.A. Gottardi, C. Gowers, B.J. Green, R. Haange, A. Haigh, C.J. Hancock, P.J. Harbour, N.C. Hawkes[7], N.P. Hawkes[1], P. Haynes[7], J.L. Hemmerich, T. Hender[7], J. Hoekzema, L. Horton, J. How, P.J. Howarth[5], M. Huart, T.P. Hughes[4], M. Huguet, F. Hurd, K. Ida[18], B. Ingram, M. Irving, J. Jacquinot, H. Jaeckel, J.F. Jaeger, G. Janeschitz, Z. Jankowicz[22], O.N. Jarvis, F. Jensen, E.M. Jones, L.P.D.F. Jones, T.T.C. Jones, J-F. Junger, F. Junique, A. Kaye, B.E. Keen, M. Keilhacker, W. Kerner, N.J. Kidd, R. Konig, A. Konstantellos, P. Kupschus, R. Lässer, J.R. Last, B. Laundy, L. Lauro-Taroni, K. Lawson[7], M. Lennholm, J.Lingertat[13], R.N. Litunovski, A. Loarte, R. Lobel, P. Lomas, M. Loughlin, C. Lowry, A.C. Maas[15], B. Macklin, C.F. Maggi[16], G. Magyar, V. Marchese, F. Marcus, J. Mart, D. Martin, E. Martin, R. Martin-Solis[8], P. Massmann, G. Matthews, H. McBryan, G. McCracken[7], P. Meriguet, P. Miele, S.F. Mills, P. Millward, E. Minardi[16], R. Mohanti[17], P.L. Mondino, A. Montvai[3], P. Morgan, H. Morsi, G. Murphy, F. Nave[27], S. Neudatchin[23], G. Newbert, M. Newman, P. Nielsen, P. Noll, W. Obert, D. O'Brien, J. O'Rourke, R. Ostrom, M. Ottaviani, S. Papastergiou, D. Pasini, B. Patel, A. Peacock, N. Peacock[7], R.J.M. Pearce, D. Pearson[12], J.F. Peng[26], R. Pepe de Silva, G. Perinic, C. Perry, M.A. Pick, J. Plancoulaine, J-P. Poffé, R. Pohlchen, F. Porcelli, L. Porte[19], R. Prentice, S. Puppin, S. Putvinskii[23], G. Radford[9], T. Raimondi, M.C. Ramos de Andrade, M. Rapisarda[29], P-H. Rebut, R. Reichle, S. Richards, E. Righi, F. Rimini, A. Rolfe, R.T. Ross, L. Rossi, R. Russ, H.C. Sack, G. Sadler, G. Saibene, J.L. Salanave, G. Sanazzaro, A. Santagiustina, R. Sartori, C. Sborchia, P. Schild, M. Schmid, G. Schmidt[6], H. Schroepf, B. Schunke, S.M. Scott, A. Sibley, R. Simonini, A.C.C. Sips, P. Smeulders, R. Smith, M. Stamp, P. Stangeby[20], D.F. Start, C.A. Steed, D. Stork, P.E. Stott, P. Stubberfield, D. Summers, H. Summers[19], L. Svensson, J.A. Tagle[21], A. Tanga, A. Taroni, C. Terella, A. Tesini, P.R. Thomas, E. Thompson, K. Thomsen, P. Trevalion, B. Tubbing, F. Tibone, H. van der Beken, G. Vlases, M. von Hellermann, T. Wade, C. Walker, D. Ward, M.L. Watkins, M.J. Watson, S. Weber[10], J. Wesson, T.J. Wijnands, J. Wilks, D. Wilson, T. Winkel, R. Wolf, D. Wong, C. Woodward, M. Wykes, I.D. Young, L. Zannelli, A. Zolfaghari[28], G. Zullo, W. Zwingmann.

PERMANENT ADDRESSES

1. UKAEA, Harwell, Didcot, Oxon, UK.
2. University of Leicester, Leicester, UK.
3. Central Research Institute for Physics, Budapest, Hungary.
4. University of Essex, Colchester, UK.
5. University of Birmingham, Birmingham, UK.
6. Princeton Plasma Physics Laboratory, New Jersey, USA.
7. UKAEA Culham Laboratory, Abingdon, Oxon, UK.
8. Universidad Complutense de Madrid, Spain.
9. Institute of Mathematics, University of Oxford, UK.
10. Freien Universität, Berlin, F.R.G.
11. Royal Institute of Technology, Stockholm, Sweden.
12. Imperial College, University of London, UK.
13. Max Planck Institut für Plasmaphysik, Garching, FRG.
14. Risø National Laboratory, Denmark.
15. FOM Instituut voor Plasmafysica, Nieuwegein, The Netherlands.
16. Dipartimento di Fisica, University of Milan, Milano, Italy.
17. North Carolina State University, Raleigh, NC, USA
18. National Institute for Fusion Science, Nagoya, Japan.
19. University of Strathclyde, 107 Rottenrow, Glasgow, UK.
20. Institute for Aerospace Studies, University of Toronto, Ontario, Canada.
21. CIEMAT, Madrid, Spain.
22. Institute for Nuclear Studies, Otwock-Swierk, Poland.
23. Kurchatov Institute of Atomic Energy, Moscow, USSR
24. Queens University, Belfast, UK.
25. Keldysh Institute of Applied Mathematics, Moscow, USSR.
26. Institute of Plasma Physics, Academica Sinica, Hefei, P. R. China.
27. LNETI, Savacem, Portugal.
28. Plasma Fusion Center, M.I.T., Boston, USA.
29. ENEA, Frascati, Italy.

At 1st July, 1992